Simultaneous Material Microstructure Classification and Discovery using Acoustic Emission Signals

by

Huifeng Sun

A Thesis Presented in Partial Fulfillment
of the Requirements for the Degree
Master of Science

Approved May 2020 by the
Graduate Supervisory Committee:

Hao Yan, Co-Chair
John Fricks, Co-Chair
Dan Cheng

ARIZONA STATE UNIVERSITY

May 2020

ABSTRACT

Acoustic emission (AE) signals have been widely employed for tracking material properties and structural characteristics. In this study, the aim is to analyze the AE signals gathered during a scanning probe lithography process to classify the known microstructure types and discover unknown surface microstructures/anomalies. To achieve this, a Hidden Markov Model is developed to consider the temporal dependency of the high-resolution AE data. Furthermore, the posterior classification probability and the negative likelihood score for microstructure classification and discovery are computed. Subsequently, a diagnostic procedure to identify the dominant AE frequencies that were used to track the microstructural characteristics is presented. In addition, machine learning methods such as KNN, Naive Bayes, and Logistic Regression classifiers are applied. Finally, the proposed approach applied to identify the surface microstructures of additively manufactured Ti-6Al-4V and show that it not only achieved a high classification accuracy (e.g., more than 90%) but also correctly identified the microstructural anomalies that may be subjected to further investigation to discover new material phases/properties.

ACKNOWLEDGMENTS

I would like to express my sincere gratitude to my advisor Dr. Hao Yan, who contributes to the instructions and supports for this thesis. I appreciate the opportunity of making a exploratory try to discover and understand on a research which will support my further study. I feel grateful to Dr. John Fricks and Dr. Dan Cheng who provide me feedback and suggestions for my thesis.

TABLE OF CONTENTS

Page

LIST OF TABLES v

LIST OF FIGURES vi

PREFACE viii

CHAPTER

1 INTRODUCTION 1

1.1 Background of Discovery of Novel Materials 1

1.2 Objective 3

1.3 Contribution 4

1.4 Further Work 5

2 EXPERIMENT DETAILS 6

2.1 Sample Preparation 6

2.2 Microstructure Analysis 7

2.3 Lithography Studies 8

3 METHODLOGY 10

3.1 Naive Bayes 10

3.1.1 Overview 10

3.1.2 Microstructure Classification 11

3.1.3 Material Discovery 13

3.2 K-Nearest Neighbors(KNN) 14

3.2.1 Overview 14

3.2.2 Microstructure Classification 15

3.2.3 Material Discovery 17

3.3 Logistic Regression 18

CHAPTER Page

3.3.1 Overview 18
3.3.2 Microstructure Classification 19
3.3.3 Material Discovery 20
3.4 Hidden Markov Model 21
3.4.1 Overview 21
3.4.2 Microstructure Classification 24
3.4.3 Material Discovery 24
3.4.4 Diagnostics for Material Discovery 24
3.5 Case Study 25
3.5.1 Problem Overview and Data Preprocessing 25
3.5.2 Results 27
3.5.3 Microstructure classification 27
3.5.4 Material Discovery 27
4 CONCLUSION 32
REFERENCES 35

LIST OF TABLES

Table Page

1. Overall Review of Naive Bayes 13

2. Overall Review of KNN 16

3. Overall Review of Logistic 20

4. Comparison among Different Classifiers 33

LIST OF FIGURES

Figure Page

1. The Ti-6Al-4V Workpiece Sample Is Mounted inside the Hysitron TI 950 Nanoindentation Setup. The AE Sensor Was Attached to the Workpiece Surface by Using Dental Cement. 3
2. (A) A Representative SEM Image of the Microstructure as Observed in the As-Fabricated Workpiece. The Microstructure Comprises of $\alpha + \beta$ Colony with α Lamellar Interspersed with Rod-Shaped β Phase. (B) A Representative Microstructure Obtained after the Polishing Was Performed on the Workpiece. The Image Shows Evidence of Extreme Coarsening of the β Phase at Scattered Locations. These Are Marked as β_W. 4
3. A Representative SEM Image of the (a) Diffused and (B) Standard Microstructure Regions Showing the Five Distinct Scratches Generated during the Lithography Process. 7
4. Confusion Matrix 11
5. Confusion Matrix for Naive Bayes 12
6. Likelihood of Naive Bayes Classifier 14
7. Testing Accuracy for KNN 15
8. Confusion Matrix for KNN 16
9. ROC Curve for KNN 17
10. Entropy for KNN 18
11. Confusion Matrix for Logistic 19
12. ROC Curve for Logistic 20
13. Entropy for Logistic 21

Figure Page

14. Illustrative Picture of HMM, the S_i's Are the Hidden or Latent State Variable and $\mathbf{O}_i$'s Are the Observed Variables 22
15. AE Sensor Signal from Frequency Domain. Ten Different Colors Represent the Diffused Microstructures and Standard Microstructures from left to Right. 26
16. Results of Material Microstructure Classification and Material Discovery. (a) Shows the Prediction Accuracy Compared the Prediction Labels (Shown in Red) with the True Labels (Shown in Black). (B) Shows the Negative Likelihood Score to Identify Each Sample Being New Material/anomaly. ... 29
17. (A) and (B) Are the Scratches that Have Been Identified as 'new Material'. (C) and (D) Are Identified as Normal Samples. As Can Be Seen from All Figures, F1 Is Always Associated the Low-Likelihood Score due to the Large Sample-To-Sample Variations. 30
18. Diagnostics Plot for Diffused V and Standard V 31
19. Discriminative vs Generative 33

PREFACE

This thesis is a try to explore a new approach to classify the known microstructure types and discover unknown surface microstructures. The data is collected from an experiment of nanolithography process by creating scratches on the surface of a given material via a diamond indenter. The data is of temporal dependency, and a hidden Markov model is applied to the data. After transforming the original data using fast fourier transformation into frequency domain, the data is splitted into 50 features, each feature representing 0-5 kHz frequency range.

The goal of our experiment is to distinguish the two surface micro-structures of Ti-6AL-4V, a titanium alloy fabricated via electron beam melting (EBM), by analyzing the acoustic emission(AE) signals collected during a nanolithography process. Furthermore, we can develop a new approach to discern intrinsic properties of materials faster, compared to conventional techniques.

I have mainly contributed to the case study part of this paper and also tried using other machine learning classification methods such as Naive Bayes, KNN, and Logistic classifiers. In addition, I am responsible for reading output from python and making some explanations of graphs. After fitting these machine learning models, we use a confusion matrix to represent the prediction ability by calculating accuracy, recall and precision. Furthermore, we evaluate the anomaly detection procedure for both generative and discriminative models and evaluate its performance.

Chapter 1

INTRODUCTION

1.1 Background of Discovery of Novel Materials

Throughout history, the process of discovering new materials has been slow, largely due to the combinatorial nature of identifying the "correct" material combination/composition as well as the time-consuming characterization tests (such as X-ray diffraction, electron microscopy) to ensure the quality and integrity of the materials. Recent breakthroughs in additive and hybrid manufacturing technologies have accelerated the fabrication of geometrically complex as well as functionally graded components Chen et al. 2015; Sames et al. 2016. However, the process of characterizing the material properties and microstructure is still slow, creating a bottleneck in the discovery of novel materials Aspuru-Guzik and Persson 2018; Alberi et al. 2018.

In recent years a major thrust has been towards developing novel approaches to enable rapid, in-situ characterization of material structure and property Pablo et al. 2014. For instance, authors in Min et al. 2005 developed a novel approach to track the deformation mechanism while performing the tensile testing by recording the ultrasonic vibrations. Such an approach allowed rapid materials characterization, potentially eliminating the need for costly experimentation such as X-ray diffraction. Along a similar direction, Iquebal, Pandagare, and Bukkapatnam 2019 utilized the capability of high-resolution acoustic emission sensing (with sampling rates exceeding 1000 kHz) and nanolithography together with machine learning to identify the microstructural fingerprint of Ti-6Al-4V. A nanolithography process essentially involves

creating scratches on the surface of a given material via the controlled motion of a diamond indenter Botcha et al. 2018. The methodology harnessed the capability of a nanoindenter to selectively probe the surface microstructures as the indenter scans through the surface. The corresponding AE response—originating from various physical transformation mechanisms such as plastic deformation, shear localization, etc.—captures the microstructural fingerprint of the material. More specifically, Iquebal, Pandagare, and Bukkapatnam 2019 showed that the AE spectrum in the range of 0.3-1 kHz and 30-50 kHz was able to distinguish different microstructure types in additively manufactured Ti-6Al-4V. AE sensing has been extensively employed in previous works. For instance, De Bono et al. 2017; Karimi, Heidary, and Ahmadi 2012 employed AE to study the strength of materials, Baccar and Söffker 2015 used AE to analyze the wear characteristics and Wisner et al. 2019; Sause et al. 2012 studied the crack propagation using AE sensing.

This cheap deployment of the AE sensors with the nanolithography process offers a great possibility for fast mapping of the microstructures with relatively lower costs and efforts. However, AE sensors produce very high-resolution time-series data with complex temporal dependency, which requires advanced data science techniques to handle. Recently, a few works have focused on analyzing the AE data. For example, classification models were developed in Iquebal, Pandagare, and Bukkapatnam 2019; Wei et al. 2018 to classify the microstructure types of the underlying material. However, despite the ability to classify known microstructures, these works failed to detect new or unknown types of materials.

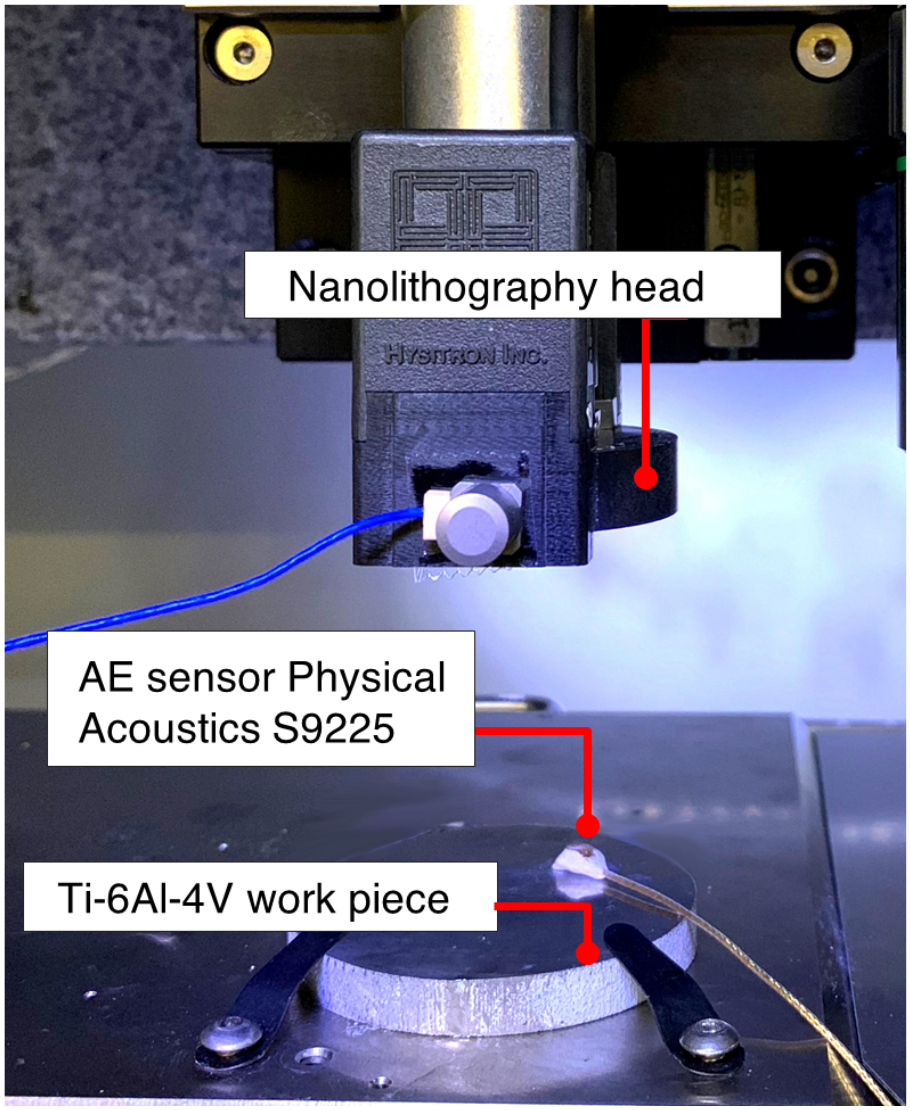

Figure 1: The Ti-6Al-4V workpiece sample is mounted inside the Hysitron TI 950 nanoindentation setup. The AE sensor was attached to the workpiece surface by using dental cement.

1.2 Objective

The objective of this work is to assess how to utilize the AE sensor data to accurately discern the microstructure types by using AE sensing of a nanolithography process while simultaneously allowing the discovery of unknown materials microstructure. To

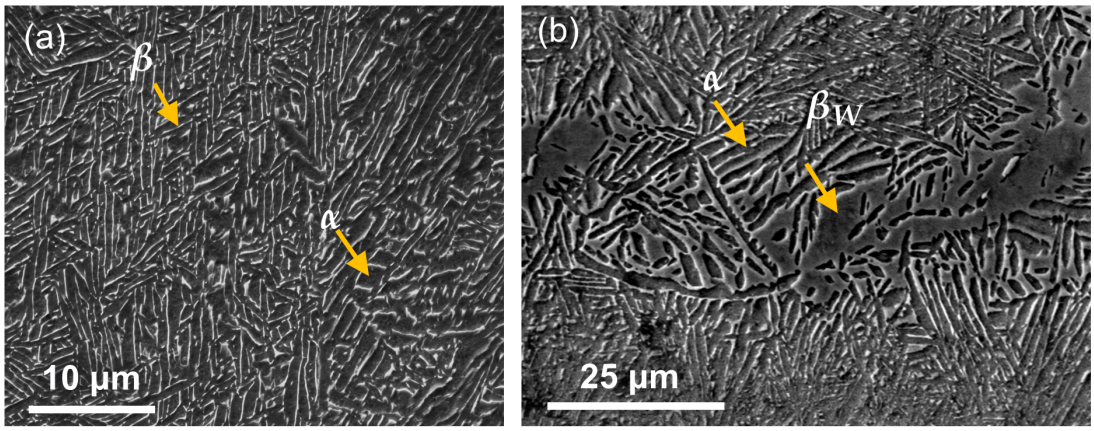

Figure 2: (a) A representative SEM image of the microstructure as observed in the as-fabricated workpiece. The microstructure comprises of $\alpha + \beta$ colony with α lamellar interspersed with rod-shaped β phase. (b) A representative microstructure obtained after the polishing was performed on the workpiece. The image shows evidence of extreme coarsening of the β phase at scattered locations. These are marked as β_W.

achieve this goal, we present a hidden Markov model (HMM) approach, which is a generative classification model considering the temporal structure of the AE signal. We further develop techniques to classify the known material microstructures and detect new material microstructures simultaneously. Here, the detected new microstructure can either be a defect on the surfaces or new types of material produced by the manufacturing processes, which require further material characterization such as SEM or XRD.

1.3 Contribution

In conclusion, the major contribution of the paper is 1) to build an HMM model for the AE signals considering the temporal consistency. 2) to classify known material microstructures using the posterior distribution of the material microstructure types given the AE signals. 3) to quantify how likely the region is "new material" by the

negative likelihood score and provide a diagnostics tool on which feature is the leading factor for this behavior.

1.4 Further Work

To validate the proposed methodology, we first present our experimental setup consisting of a nanoindentation setup to collect AE signals during the lithography process on the Ti-6Al-4V sample surface fabricated via additive manufacturing. Then, we will present the proposed modeling framework to discriminate different material microstructures as well as detecting if any particular region belongs to any known microstructure by the negative likelihood score. Further diagnostics tools are proposed to understand which feature is the leading factor of such behavior. We will give a case study on how the proposed framework is used to discover a potential "new material region" in our real experiments. Finally, we will conclude the paper with the conclusions and future works.

Chapter 2

EXPERIMENT DETAILS

Scanning probe lithography referred to as lithography in the rest of the manuscript employs a nanoindentation tool for texturing patterns on the surface of a given material. As a result of selectively probing the surface, the lithography process offers an approach to rapidly track the microstructural fingerprint of the material under investigation Chang and Bukkapatnam 2004 by recording the micro-elastic pulses generated as the indenter scans the surface. In this section, we present the description of sample fabrication and preparation, microstructure details, lithography experiments, and data collection.

2.1 Sample Preparation

In the present work, we perform the lithography on Ti-6Al-4V workpiece samples fabricated using an electron beam melting (EBM) process. The as-fabricated workpiece was subsequently subjected to a multi-step finishing process on a hand-held Buehler Metaserv grinder-polisher (model 95-C2348-160). The finishing process employed Silicon Carbide (SiC) polishing pads with progressively reducing abrasive sizes (600 grits to 1200 grits). To impart a specular finish ($S_a \leq 25$ nm), the surface was finally polished using alumina abrasives of size 0.05 μm suspended in an aqueous solution with abrasive concentration at 20% by weight and pH ≈ 7.5. Throughout the polishing process, a nominal down pressure of 0.5kPa was maintained. The polisher was set to 500 revolutions per minute while ensuring a quasi-random motion. To observe

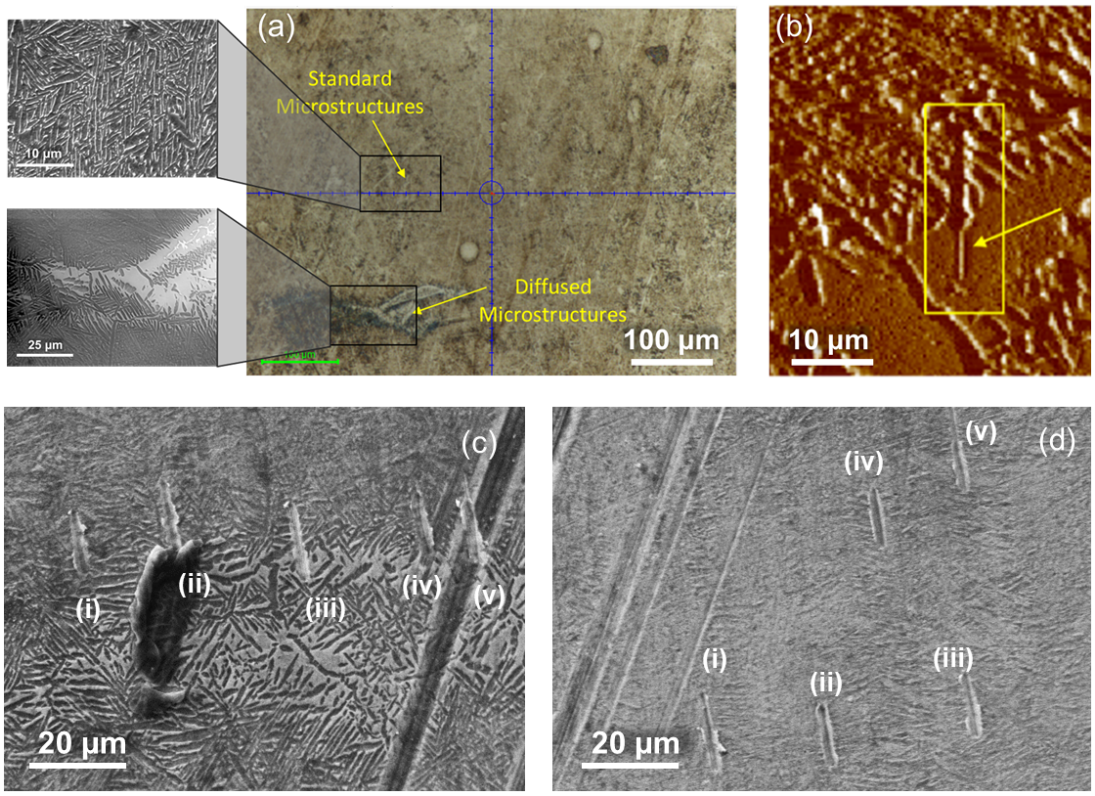

Figure 3: A representative SEM image of the (a) diffused and (b) standard microstructure regions showing the five distinct scratches generated during the lithography process.

the microstructures, the polished surface was etched with Kroll's reagent ($5-7\%$ nitric acid, $2-4\%$ hydrofluoric acid, and rest distilled water) for 10 seconds and rinsed thoroughly with distilled water. The microstructure was then observed under a scanning electron microscope (SEM) under high vacuum conditions.

2.2 Microstructure Analysis

The polished surface comprised of standard α and β microstructures organized in colonies as well as basket-weave morphology. A representative SEM image of the microstructure is shown in Figure 2(a) with lamellar α phase in gray and the rod-

shaped β phase in white. For modeling purposes, we refer to this $\alpha + \beta$ microstructure as the "standard microstructure". From a quantitative standpoint, the standard microstructure is primarily comprised of ∼90% α phase with ∼10% β phase.

A recent study has shown that mechanical polishing of as-fabricated Ti-6Al-4V workpiece under dry conditions result in the dilation of the β phase due to high temperatures (in the range of 700-1000 K) at the asperity-abrasive contacts during polishing Iquebal, Sagapuram, and Bukkapatnam 2019. We refer to this microstructure type, with widened β phase, as the diffused microstructure. This is labelled as β_W in Figure 2(b) and is composed of roughly 60% α and 40% β. Such non-equilibrium microstructures offer a unique potential to tailor the mechanical behavior of the workpiece such as the hardness and tensile strength of additively manufactured components for specific applications Wang, Palmer, and Beese 2016.

2.3 Lithography Studies

In this work, lithography studies were performed on a sensor integrated nanoindentation setup consisting of a Hysitron TI 950 Triboindenter carrying a Berkovich indenter with a diamond tip with tip specification as: included angle – 142.3°, tool tip radius – 100 nm, and maximum allowable downforce - 10,000 μN. The effect of external disturbances is attenuated by installing a vibration isolating platform underneath. To perform lithography experiments, three locations on the surface were identified via SEM. Each of these three locations consisted of standard and diffused microstructure types. Five parallel scratches were created at each of the standard and diffused microstructure regions and representative SEM images are shown in Figures 3(c & d). The scratches are marked as (i), (ii), (iii), (iv), and (v) and are

each of length 15 μm. The length of the scratch was selected to 15 μm to ensure that most of the primary microstructural features were scanned by each of the scratches such as the widths of the rod-shaped β and the diffused β_W phases. The indenter speed was set to 0.5 μm/sec, such that each scratch lasted for 30 sec. The AE released during the process was collected using a S9225 AE sensor from Physical Acoustic Corp with a sampling frequency of 300-1800 kHz. The aforementioned lithography process was repeated at three random locations, each containing predetermined diffused and standard microstructures, as depicted in Figure 3(a).

Chapter 3

METHODLOGY

In this work, we propose a framework to classify the known underlying microstructure of the material and identifying defects or unknown microstructure based on signals from AE sensors. To achieve this, we evaluate Naive Bayes, KNN, logistic regression, and hidden Markov model (HMM) to achieve both goals. We will first give a brief introduction of the these machine learning models and then discuss how to use each model for both known microstructure classification and unknown microstructure detection.

3.1 Naive Bayes

3.1.1 Overview

Naive Bayes is a generative classification model, which is widely used in classification based on Bayes' Rule. Recall the definition of Bayes' Rule:

$$P(y|x) = \frac{P(x|y)P(y)}{P(x)}$$

The assumption of this model is that each feature is independent, the present existing feature does not have any effect on the other. Thus, the Bayes' Rule becomes

$$P(y|x) = \frac{P(x|y)P(y)}{P(x)} = \frac{P(y)}{P(x)} \prod_{i=1}^{d} P(x_i|y).$$

The two-way table where the columns represent predicted Y and rows represent observed Y is called a confusion matrix.

		Predicted Value	
True Condition		Positive (+)	Negative (-)
	Positive (+)	True Positive (TP)	False Negative (FN)
	Negative (-)	False Positive (FP)	True Negative (TN)

Figure 4: Confusion Matrix

Accuracy, recall, precision and F-score can be calculated from the confusion matrix. The mathematical definitions are as following:

Accuracy

$$Accuracy = \frac{TP + TN}{Total}$$

Recall

$$Recall = \frac{TP}{TP + FN}$$

Precision

$$Precision = \frac{TP}{TP + FP}$$

F-score

$$F - score = \frac{2 * Recall * Precision}{Recall + Precision}$$

Recall shows the ability to find all relevant instances; Precision shows the proportion of data points our model says was relevant actually were relevant. We expect both high recall and high precision, but it is not the case usually. So we use F-score to trade-off which measures Recall and Precision at the same time.

3.1.2 Microstructure Classification

To meet the assumptions of Naive Bayes classifier, we assume each feature in our data are conditionally independent given each classification and do not have any effect

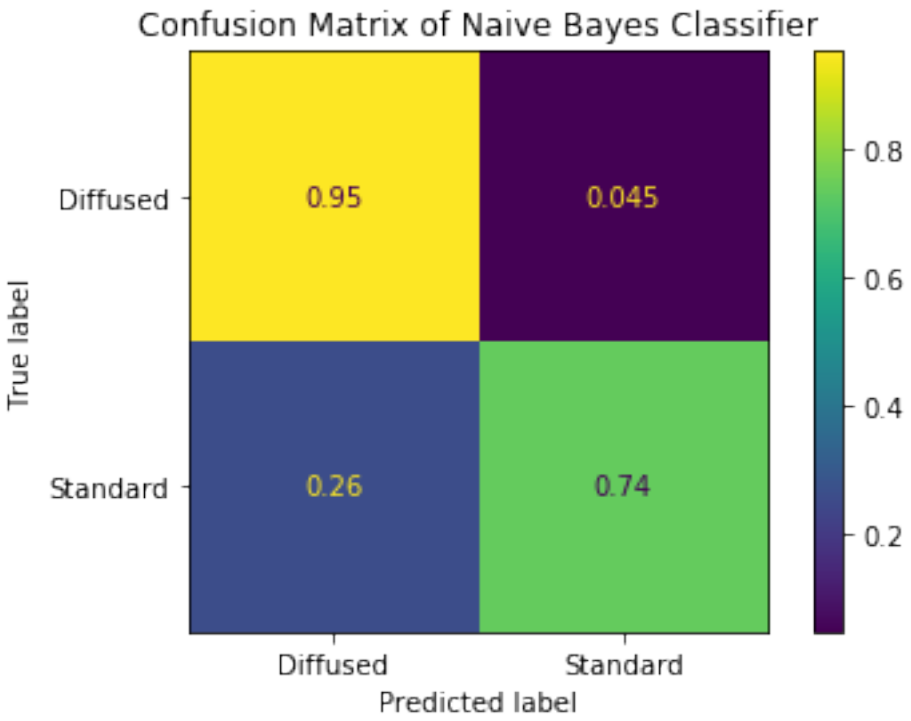

Figure 5: Confusion Matrix for Naive Bayes

to each other. In addition, data given each classification are assumed to be generated from Gaussian process and thus are normally distributed.

After fitting the Naive Bayes model to our data, we plot the confusion matrix and further calculate precision, accuracy, recall, etc to evaluate our model.

From the confusion matrix, we can conclude the probability of predicting diffused microstructures when they are actually diffused is 0.95 and the probability of predicting standard microstructures when they are actually standard is 0.74.

From the results of the Naive Bayes model, the precision of predicting diffused microstructures is 0.78 and of predicting standard microstructures is 0.94. The recalls are 0.95 and 0.74 and f1-scores are 0.86 and 0.83 accordingly. Though some differences between the precisions and the recalls, f1-scores look well.

The accuracy score in this case is 0.85 which is not a concern. Thus, our Naive Bayes model fits nicely on our dataset and has good prediction probability.

Table 1: Overall Review of Naive Bayes

	precision	recall	f1-score
Diffused	0.78	0.95	0.86
Standard	0.94	0.74	0.83

3.1.3 Material Discovery

The likelihood of X is defined as

$$P(X) = 1/2 * P(X|Y = 0) + 1/2 * P(X|Y = 1).$$

The likelihood reflects how well the model can explain our data and detect anomalies.

In our data, two classifications are known: diffused microstructures and standard microstructures. However, some points are predicted with low likelihood and imply undefined structures existing. This helps us to detect new material characterization and discover new material.

The likelihood of the Naive Bayes model shows data samples from 900-1100, originally standard V phrase, are predicted with low probability to be either diffused or standard microstructures and thus are assumed to be new materials.

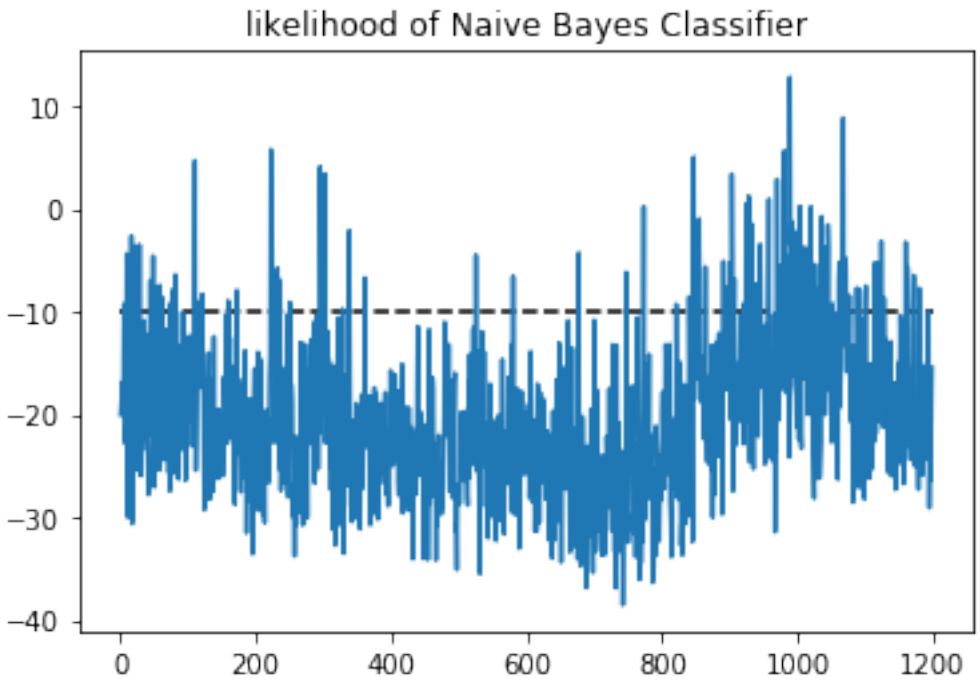

Figure 6: Likelihood of Naive Bayes Classifier

3.2 K-Nearest Neighbors(KNN)

3.2.1 Overview

K-Nearest Neighbors is a discriminative classifier in machine learning models and can be used for both classification and regression. The KNN algorithm assumes things with similar features are near each other and thus captures similarities by measuring distance among points.

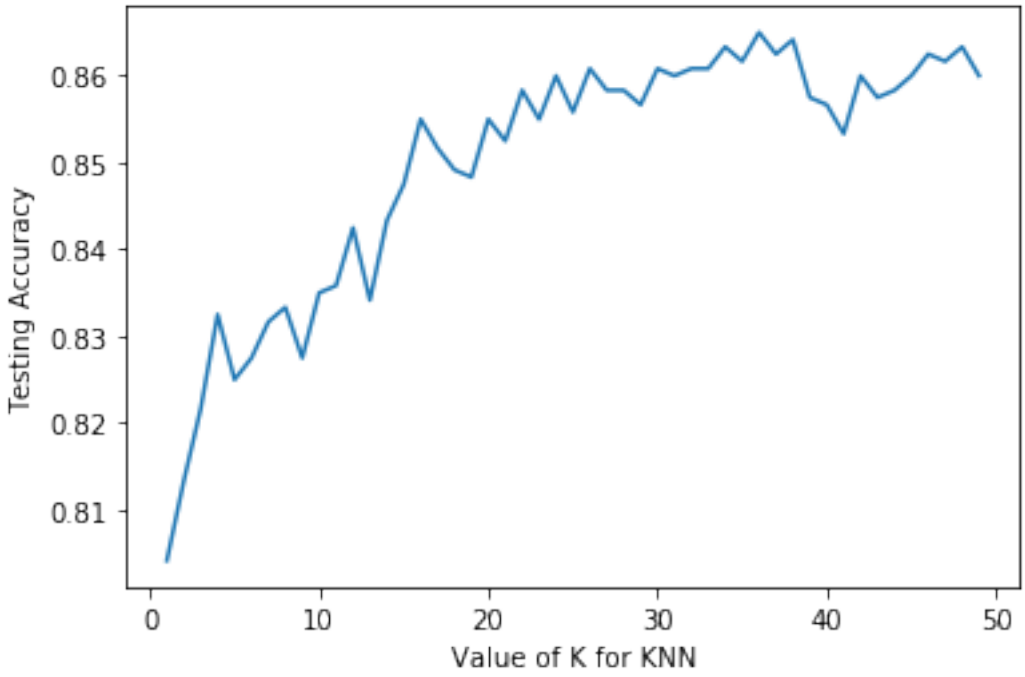

Figure 7: Testing Accuracy for KNN

3.2.2 Microstructure Classification

First, we fit the KNN models to our data and calculate the accuracy scores with different ks. From the line chart and accuracy scores results, we safely choose k equals to 30 with about 96% accuracy.

The confusion matrix of KNN gives us an initial intuition about the prediction ability. Besides, the precision is 0.97 and the recall is 0.94 for diffused microstructures. The precision is 0.95 and the recall is 0.97 for standard microstructures. The difference between precision and recall is very small, and f1-score is 0.96, so we expect the prediction ability quite well. The ROC curve looks nearly perfect with the AUC score equals to 0.99.

The accuracy score in KNN model is 0.96 which means the predicted classifications

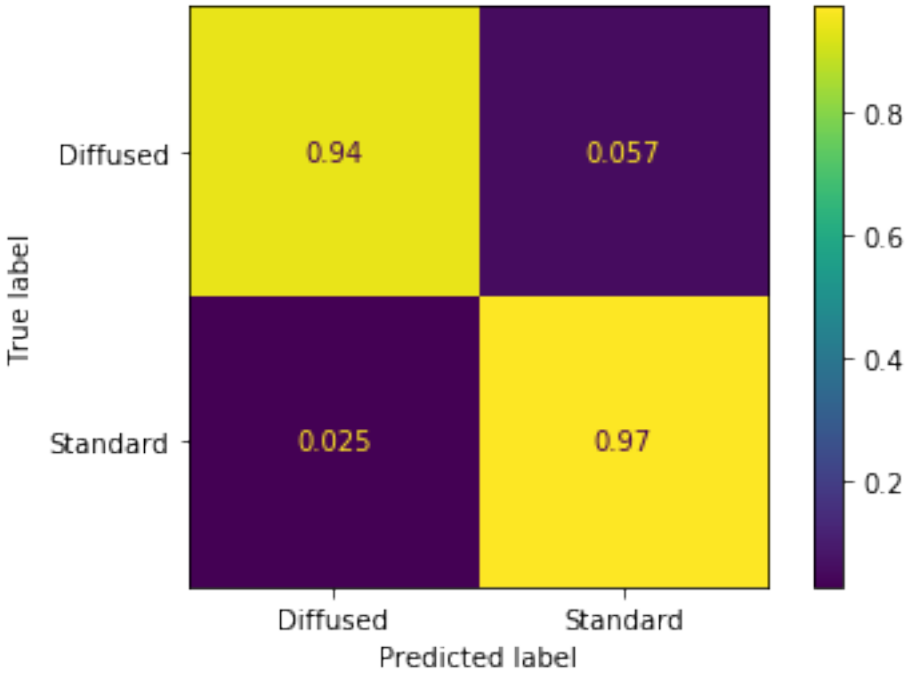

Figure 8: Confusion Matrix for KNN

are quite reliable and accurate. All these metrics prove that KNN is a good model to do classification in our data.

Table 2: Overall Review of KNN

	precision	recall	f1-score
Diffused	0.97	0.94	0.96
Standard	0.95	0.97	0.96

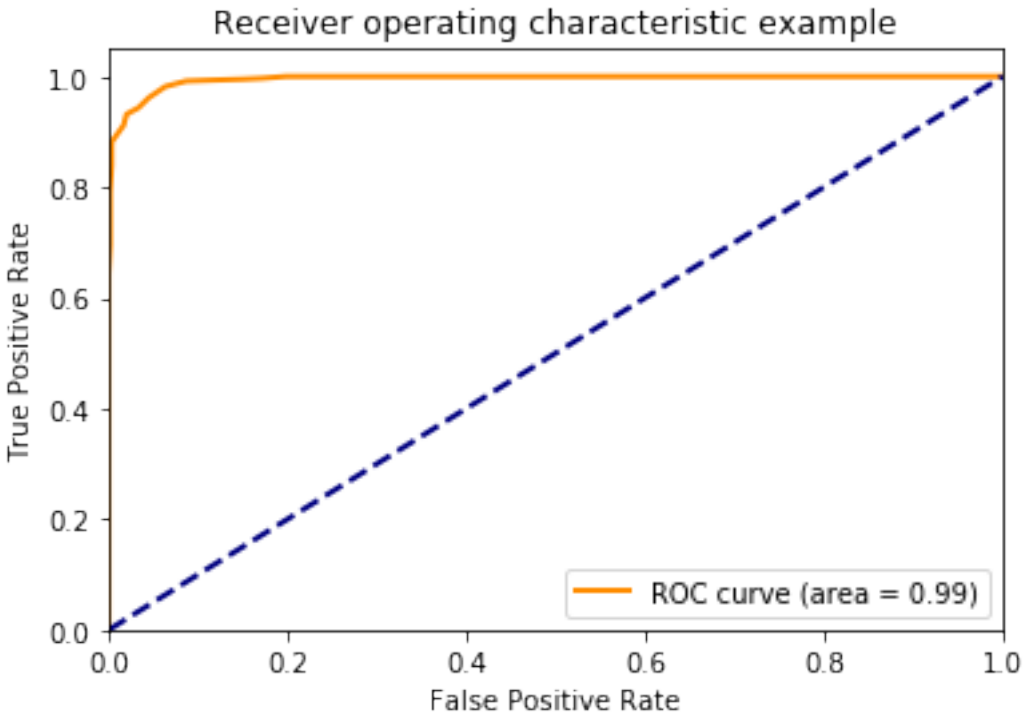

Figure 9: ROC Curve for KNN

3.2.3 Material Discovery

Entropy is a measurement of uncertainty used in discriminative classifiers. Entropy H is mathematically defined as:

$$H = -p * logp - (1-p)log(1-p).$$

P is the probability when diffused microstructures occur.

To find unknown classification, the entropy of KNN shows the points from 360 to 700,where is diffused III located, and 1100 to 1200, where is standard V located, are anomalies. These points are predicted neither diffused nor standard and are assumed to be new materials that never appear in our training data.

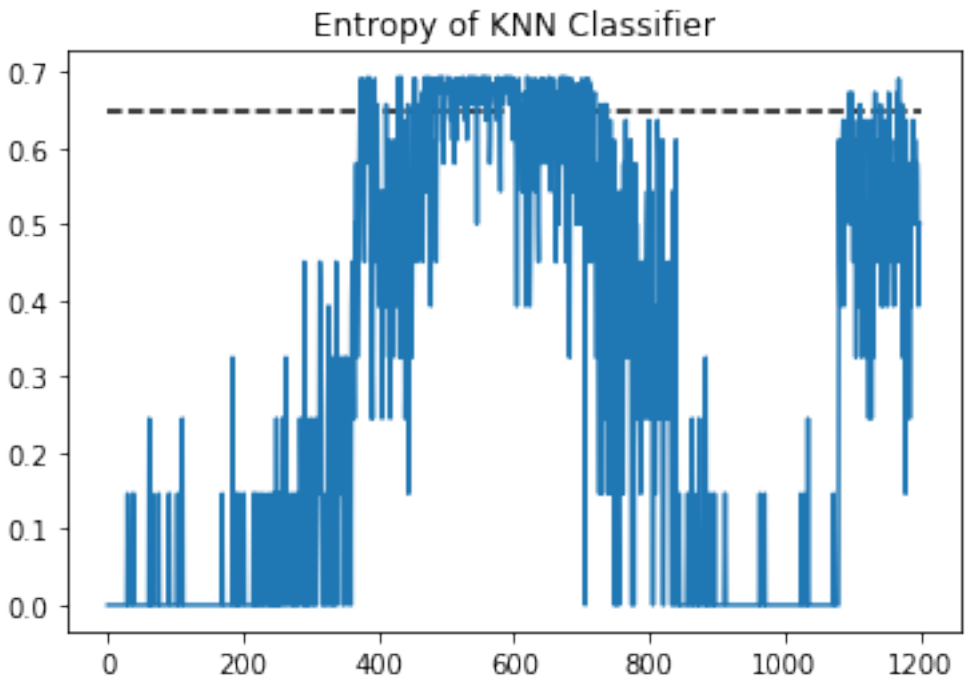

Figure 10: Entropy for KNN

3.3 Logistic Regression

3.3.1 Overview

Logistic Regression is another discriminative classifier in machine learning models. It is a method used in the situation when response variable is categorical. Logistic function, known as sigmoid function, is a monotonic, continuous function bound between 0 and 1 with S shape. The function is defined as

$$y = \frac{exp(\beta X)}{1 + exp(\beta X)}.$$

y is 0 if the microstructure is diffused and is 1 if microstructure is standard in our model.

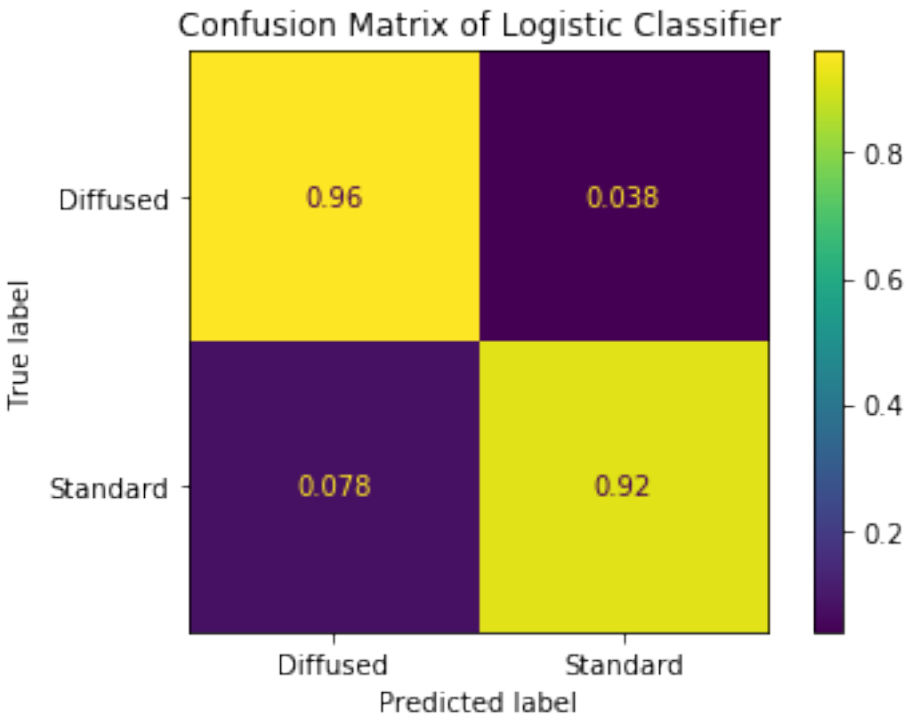

Figure 11: Confusion Matrix for Logistic

3.3.2 Microstructure Classification

The accuracy of logistic prediction is 0.95 which is pretty high so we can trust the prediction results to large extent. The precision and recall for diffused microstructures are 0.95 and 0.96 separately, and are 0.96 and 0.95 for standard microstructures separately. The f1-score is 0.95 for both classifications.

The ROC curve looks similar to the previous two which has nearly perfect look with very high AUC score equaling to 0.99. So out logistic regression model is very good at distinguishing two difference microstructures.

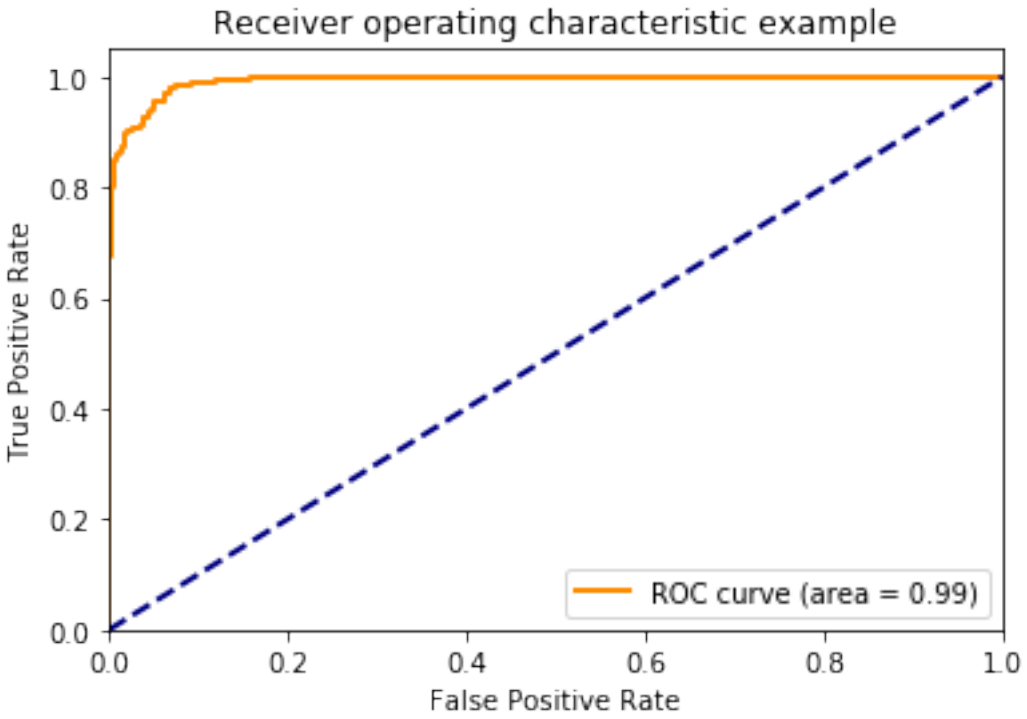

Figure 12: ROC Curve for Logistic

Table 3: Overall Review of Logistic

	precision	recall	f1-score
Diffused	0.95	0.96	0.95
Standard	0.96	0.95	0.95

3.3.3 Material Discovery

The entropy of logistic classifier shows that the data points from 500 to 700,diffused IV, and 1100 to 1200,standard V, have large uncertainty. So these points are assumed to be unknown materials.

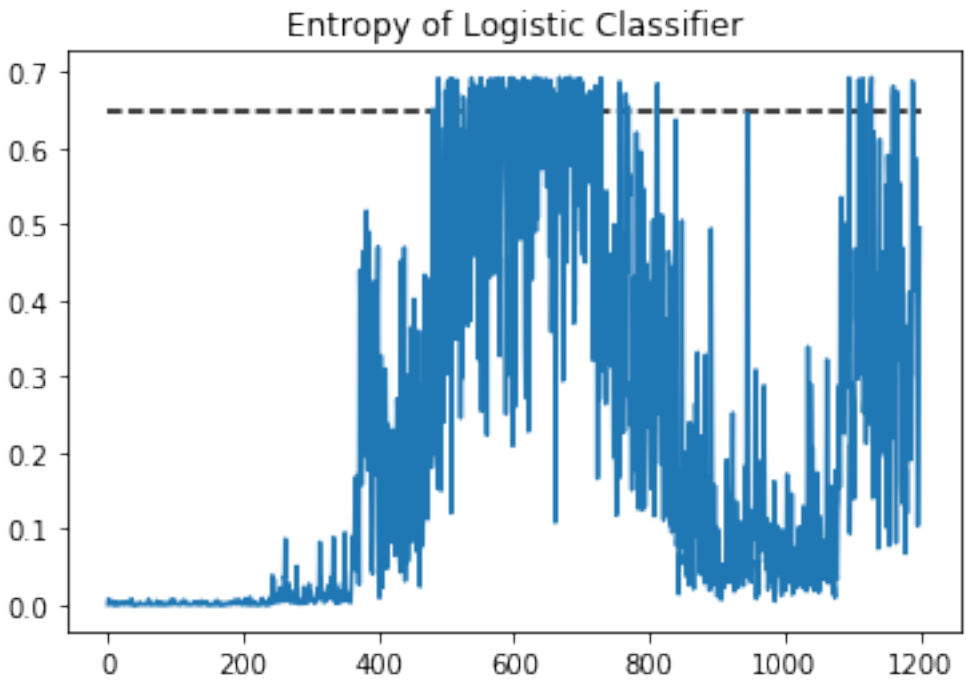

Figure 13: Entropy for Logistic

3.4 Hidden Markov Model

3.4.1 Overview

HMM is a probabilistic model that describes the transitions of a finite number of states over time. These states characterize two stochastic processes: the hidden state transition in the discrete-time and observed process. In addition, three sets of probability distributions are utilized to characterize the system dynamics: the initial probabilities for all the hidden states; the transition probabilities between two hidden states, and the emission probabilities of an observation from a hidden state. The elements of an HMM are defined as follows:

- 1) Let $\mathbf{Q} = \{1, \cdots K\}$ denote the set of hidden states, with the total number

of states to be K. We denote $S_{i,t} \in \mathbf{Q}$ as the system state at time t for unit $i \in \{1, \cdots, n\}$. Furthermore, we denote $S_{i,t}^k$ as a binary variable according to whether the system for unit i at state k in time t.

- 2) A transition probability matrix is defined as $\mathbf{A} = \{p_{kk'}\}$, in which $p_{kk'}$ is the transition probability that the system state is changed from state k to state k', $k, k' \in \{1, \ldots, K\}$ at time t,

$$p_{kk'} = P(S_{i,t+1} = k | S_{i,t} = k'), 1 \leq k, k' \leq K. \tag{3.1}$$

- An emission probability is defined on multi-variate response $\mathbf{O}_{i,t}$ by two sets of matrix $\mathbf{B} = \{\boldsymbol{\mu}_k, \boldsymbol{\Sigma}_k\}$, in which $\boldsymbol{\mu}_k$ is the mean of multiple sensors in state k, and $\boldsymbol{\Sigma}_k$ denote the covariance matrix of multiple sensing measurement. In other words,

$$\begin{aligned} (\mathbf{O}_{i,t} | S_{i,t} = k) \sim & N(\boldsymbol{\mu}_k, \boldsymbol{\Sigma}_k), \\ & i = 1, \cdots, n, k = 1, \cdots, K. \end{aligned} \tag{3.2}$$

- An initial state vector $\boldsymbol{\Pi_i} = \{\pi_{i,k}\}$ is defined to express the distribution of the system states for unit i at state k at $t = 1$.

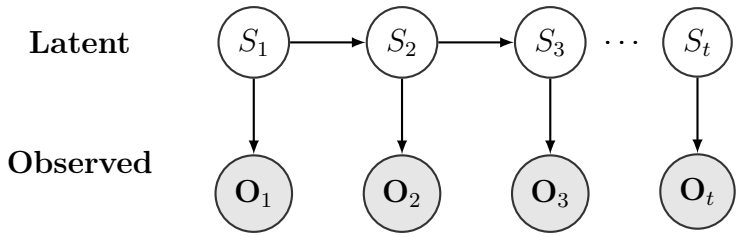

Figure 14: Illustrative picture of HMM, the S_i's are the hidden or latent state variable and $\mathbf{O}_i$'s are the observed variables

With the descriptions shown above, for the simplicity and clarification, the full HMM model is given by $\Lambda = \{Q, A, B, \boldsymbol{\Pi_i}\}$. Figure 14 shows the logical dependencies

among different random variables of an HMM. Furthermore, three major problems can be solved by the HMM Rabiner 1989:

- 1) *Evaluation problem*- Given an HMM Λ and an observation sequence $\{\mathbf{O}_{i,t}\}_{t=1}^{T} = (\mathbf{O}_{i,1}, \mathbf{O}_{i,2}, \ldots, \mathbf{O}_{i,T})$, find the probability that the sequence $\{\mathbf{O}_{i,t}\}_{t=1}^{T}$ is accrued, or $P(\{\mathbf{O}_{i,t}\}_{t=1}^{T}|\Lambda)$, using the HMM modeling. The evaluation problem an be used to evaluate both the sequence likelihood $P(\{\mathbf{O}_{i,t}\}_{t=1}^{T}|\Lambda)$ and the individual point likelihood $P(\{\mathbf{O}_{i,t}\}|\Lambda)$

- 2) *Decoding problem*- Given an HMM Λ and an observation sequence $\{\mathbf{O}_{i,t}\}_{t=1}^{T}$, identify the system state at each time t or estimate $P(S_{i,t}|\{\mathbf{O}_{i,t}\}_{t=1}^{T})$. The decoding problem will be related to the microstructure identification process.

- 3) *Learning problem*- Find the parameters in the model Λ (the $\mathbf{A}, \mathbf{B}, \mathbf{\Pi_i}$) that maximize the probability $P(\{\mathbf{O}_{i,t}\}_{t=1}^{T}|\mathbf{A}, \mathbf{B}, \mathbf{\Pi_i})$.

For more details of using the Expectation-Maximization algorithms and the forward-backward algorithms to solve these three problems, please refer to Rabiner 1989. We will then review how to use the three problems to solve the problems of microstructure classification and new material discovery. First, the parameters of the HMM models need to be learned by solving the learning problem. Then we propose to use the decoding problem and evaluation problem to solve the problem of microstructure classification and material discovery.

3.4.2 Microstructure Classification

We propose to differentiate known underlying material microstructures by solving the decoding problem in HMM. With model parameters determined, we are able to classify the observation by solving a decoding problem to find the probability $P(S_t = k|\{O_t\}_{t=1}^T)$. The decoding problem is used solved through the Forward-backward algorithm by decomposing the equation into two terms $P(O_1, ..., O_t, S_t = k, O_{t+1})$ and $P(O_{t+1}, ..., O_T|S_t = k)$, and solve both terms using the dynamic programming. Here, we will classify the microstructure according to the largest posterior distribution $\hat{k}_t = \arg\max_k P(S_t = k|\{O_t\}_{t=1}^T)$

3.4.3 Material Discovery

Given the trained HMM Λ, we denote the sequence with low likelihood $P(O_1, O_2, ..., O_t|\Lambda)$ as the sequence with potential new material. We can also calculate the likelihood for a single point $P(\{\mathbf{O}_{i,t}\}|\Lambda)$ by summing up all possible states $\sum_{j=1}^K P(O_t|S_t = j)$. In this way, the problem of material discovery can be solved by the evaluation problem in HMM.

3.4.4 Diagnostics for Material Discovery

We further analyze which feature is the leading factor that the HMM quantifies the sequence as the "new material" sequence. To achieve this, we find that under the assumption that the covariance matrix of the emission is a diagonal matrix, the likelihood score can be decoupled into the likelihood of each individual feature. For

example, if we know that all features O_{tj} of observation at time t are independent, the log-likelihood can be decoupled as following:

$$\log P(O_t|\Lambda) = \sum_j \log P(O_{tj}|\Lambda) \tag{3.3}$$

O_{tj} represents the jth feature of observation O_t. With this decoupled likelihood, we are able to calculate the likelihood of each feature seperately.

3.5 Case Study

3.5.1 Problem Overview and Data Preprocessing

Finally, we will apply the proposed methodology to the real case study. The acoustic emission (AE) signals are collected from a nanolithography process, described in the experimental setup. We have collected five parallel scratches from the three locations. For each scratch, it is divided into segments with 0.25s. with 125000 $(= 0.25 \times 500,000)$ data points. Each of these segments is labeled as either diffused and standard microstructure. Therefore, we have in total 600 $(= 30\text{sec} \times (1/0.25\text{sec}) \times 5.$) samples from each class of microstructure.

We further preprocess the AE sensor signal in the following data processing pipeline:

- 1) Each time slice was transferred into the Fourier domain with 62500 data points for each set. As the sampling rate of the AE data was 500 kHz, the frequency range of 0-250 kHz could only be observed.
- 2) The entire frequency band is further divided into 50 non-overlapping intervals (each representing a frequency range of 5 kHz.

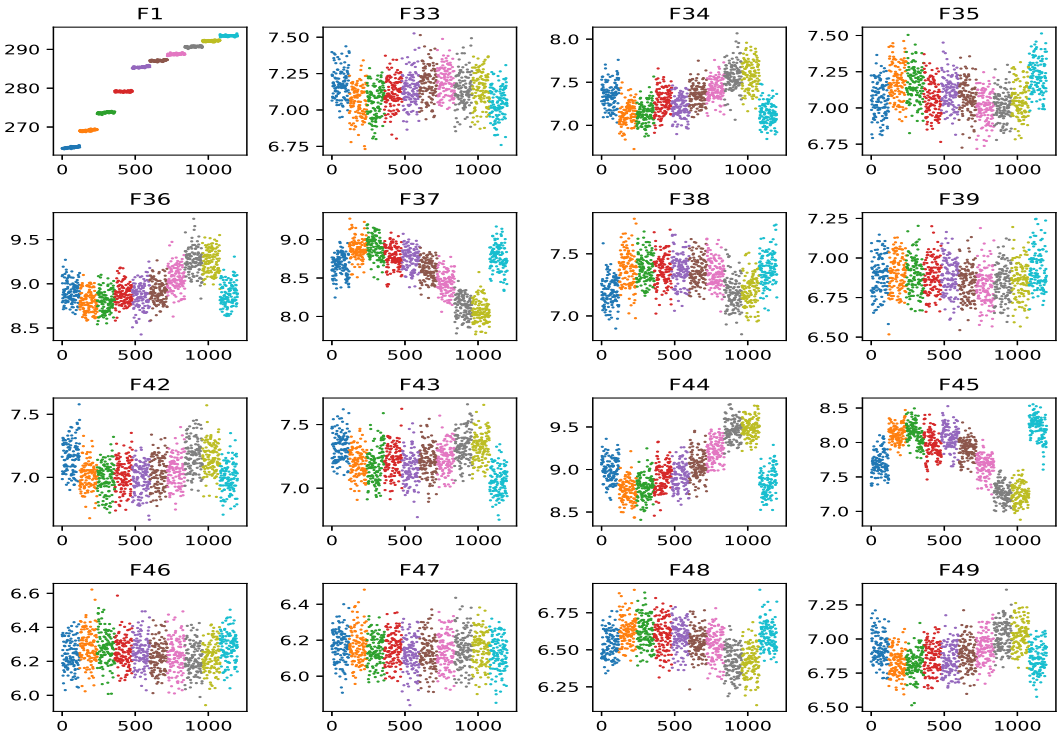

Figure 15: AE sensor signal from frequency domain. Ten different colors represent the diffused microstructures and standard microstructures from left to right.

- 3) The root mean square values of the power in each of these intervals are calculated as features.

After the preprocessing, the dataset comprises 600 sample observations and 50 features for each class (Standard/ Diffused) on each location. Fig. 15 shows several selected frequency bands (e.g. F1, F33-F50) of AE sensor signal. The different color shows the samples from different scratches. The first five scratches are diffused phase, and the last five are standard phases.

From Fig. 15, it seems that F1 is very sample-dependent since all ten scratches share very different F1 features. Furthermore, standard V (e.g., shown in the light blue color) has very different F44 and F45 values.

3.5.2 Results

3.5.3 Microstructure classification

For the microstructure classification, Table. xxx shows the classification results (precision, recall, F1-score, AUC) from RF, NB, and HMM. From the results, we can see that we are able to classify most of the sequences except Diffused V. We further calculate the likelihood of each sequence and present the results as Fig. 3.16(b). We can find that Diffused V got the wrong prediction, which is due to that this Diffused V gets a very low likelihood score compared to others. In order to understand the reason for it, we did a diagnostic process by decomposing the likelihood score of a sequence into the likelihood score of the features of the sequence. To report the accuracy, we can conclude that all standard structures are predicted correctly and diffused structures are predicted correctly except diffused V.

3.5.4 Material Discovery

Fig. 3.16(b) shows the sequence of negative likelihood among ten observed locations. From this figure, we see that diffused V, standard IV, and standard V locations will have a lower likelihood than other locations. Among these, diffused V has the lowest likelihood score. The lower likelihood score shows that the model is not very confident in modeling these scratches, partially due to that these scratches are different from others.

Both Fig. 3.17(a) and Fig. 3.17(b) are identified as the "new material", the likelihood

score of diffused phase is much smaller than that of the standard phase of feature 'F1', so feature 'F1' is a quite important factor which influences the prediction results. These two plots are consistent with the results showed from the sequence likelihood in Fig. 3.16(b). Furthermore, the overall likelihood score for diffused and standard are smaller, which contributes to the decision of "new material". For Diffused V, this finding is consistent with the SEM images reported as shown in Fig. 3.18(a), where Diffused V seems to be in a slightly darker region and the 'F1' frequency is much closer to the standard material. For Standard V, 'F45' shows as the second important feature contributing to the low overall likelihood score. This can be seen from Fig. 3.18(b), where both 'F43' and 'F45' have very different frequency features from the rest and SEM images show a slightly darker region on the Standard V. For Diffused IV and Standard II are both detected as the "normal material" and classified correctly. Interesting, we can see that despite that 'F1' is still the leading factor for the classification. F32-F45 are also important factors that contribute to the classification and material discovery decision. These findings are in alignment with the findings in Iquebal, Pandagare, and Bukkapatnam 2019.

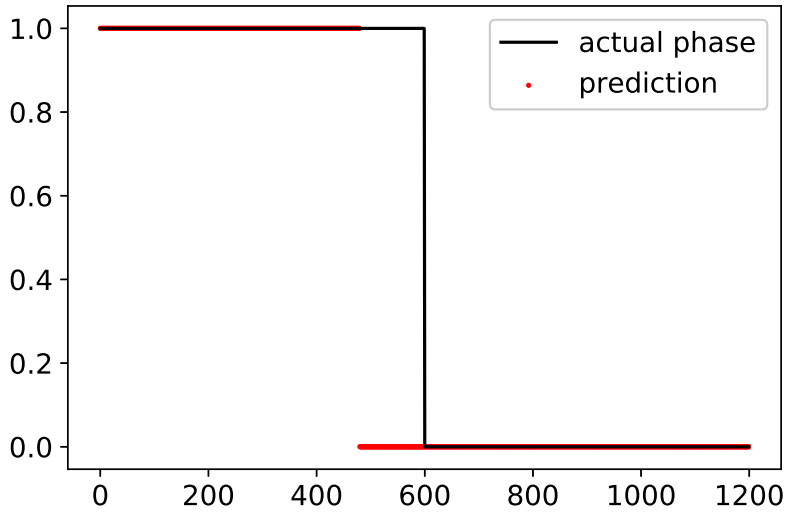

(a) Prediction Accuracy

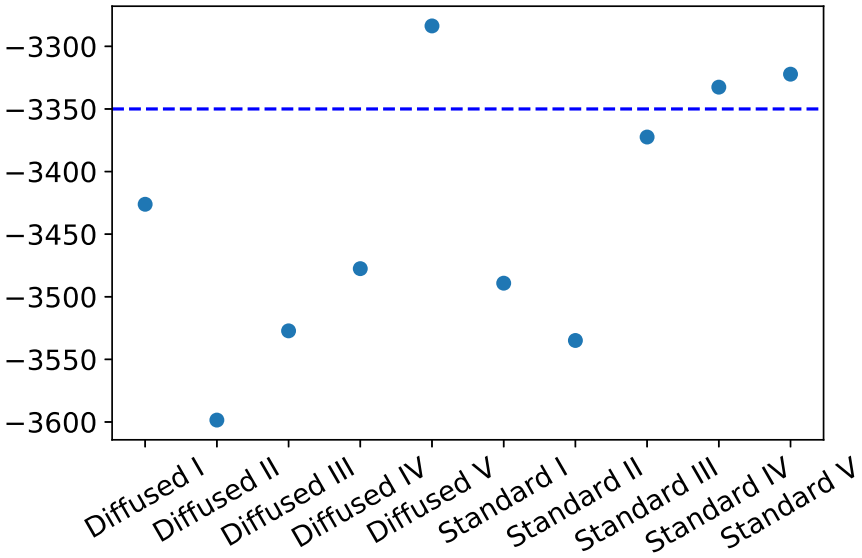

(b) Negative Likelihood Socre of Each Sample

Figure 16: Results of Material Microstructure Classification and Material Discovery. (a) shows the prediction accuracy compared the prediction labels (shown in red) with the true labels (shown in black). (b) shows the negative likelihood score to identify each sample being new material/anomaly.

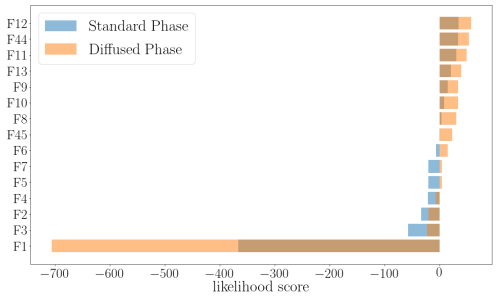

(a) Diagnostic for Diffused V

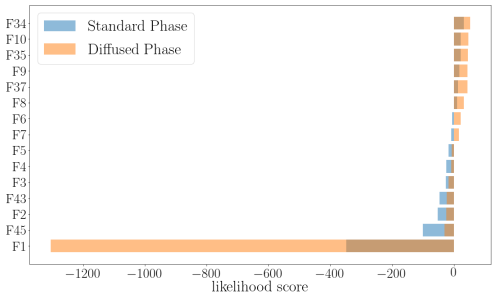

(b) Diagnostic for Standard V

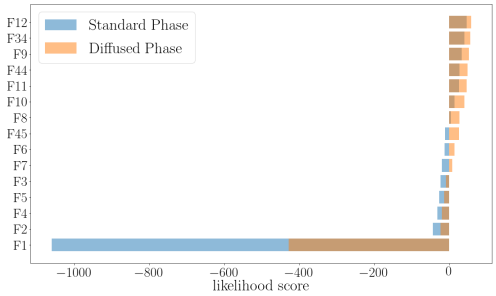

(c) Diagnostic for Diffused IV

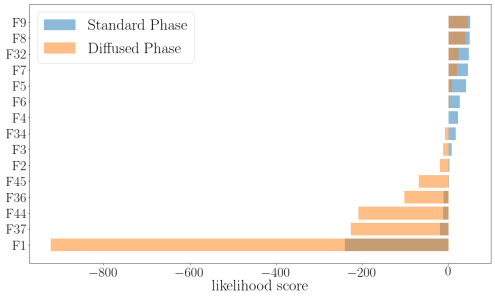

(d) Diagnostic for Standard II

Figure 17: (a) and (b) are the scratches that have been identified as 'new material'. (c) and (d) are identified as normal samples. As can be seen from all figures, F1 is always associated the low-likelihood score due to the large sample-to-sample variations.

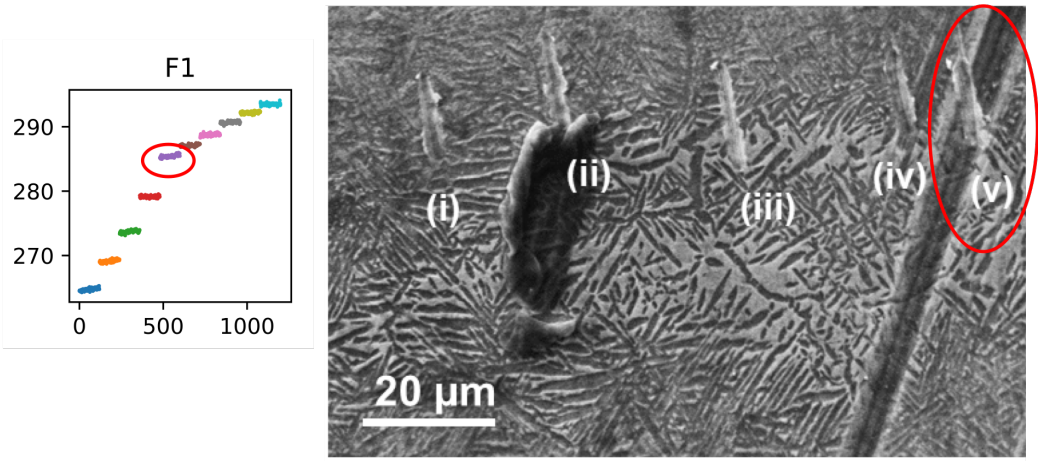

(a) Diffused V

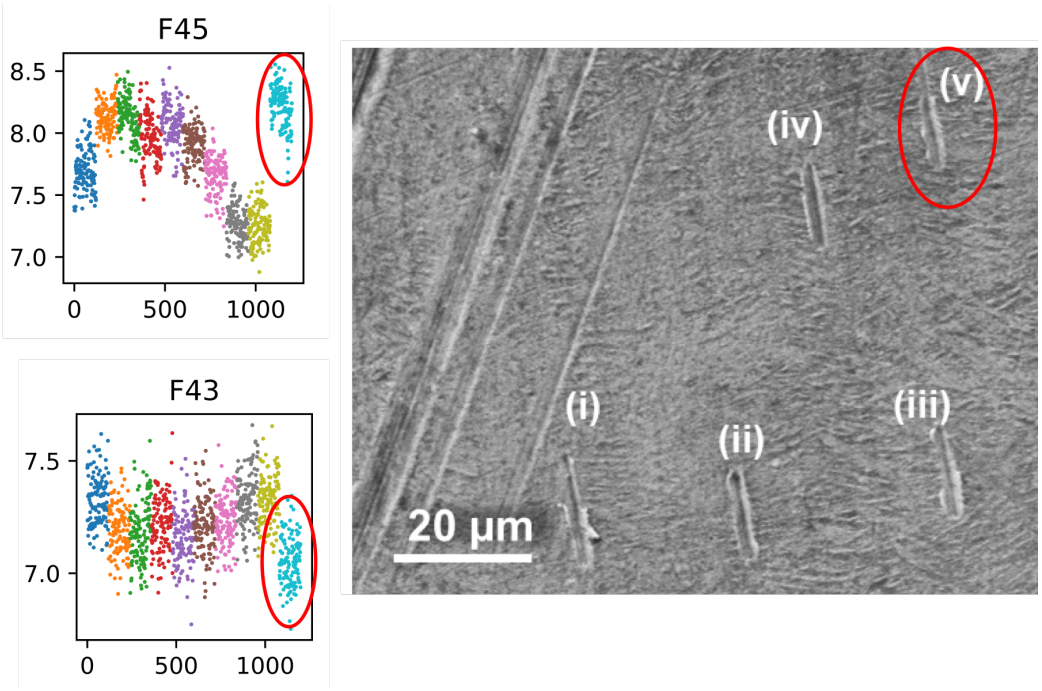

(b) Standard V

Figure 18: Diagnostics plot for Diffused V and Standard V

Chapter 4

CONCLUSION

In this work, we analyzed the acoustic emission signals generated from a lithography process for material microstructure classification and new materials discovery. In order to achieve these two objectives we propose a pipeline to extract the important frequency features from the raw signals and model the sequential data with Hidden Markov Model. We also discussed three possible applications of Hidden Markov Model. Firstly, we are able to differentiate different microstructure by solving an evaluation problem in HMM. Our results show that we can capture all sequences except one sequence. We further discover that this sequence is potentially a new material microstructure/phase due to the low likelihood score. We further confirmed this finding with the SEM images. Finally, we conduct a diagnosis process on all sequences by decomposing the log-likelihood of HMM. Through the process, we find that the root cause of diffused V being identified as the new material is due to the F1 feature.

While the proposed method is not supposed to replace the traditional high-fidelity measurements such SEM or XRD, it offers an approach to rapid gather low-fidelity information about the material microstructure that can be used as a guide to search for novel materials, therefore, significantly reducing the experimental efforts. In the future work, we will study how to combine both AE signals (low-fidelity) and SEM images or XRD (high-fidelity) for efficient material discovery.

The results of each classifier are shown in the Table: 4. KNN and logistic classifiers have a better accuracy score and f1-score compared to other two models. The

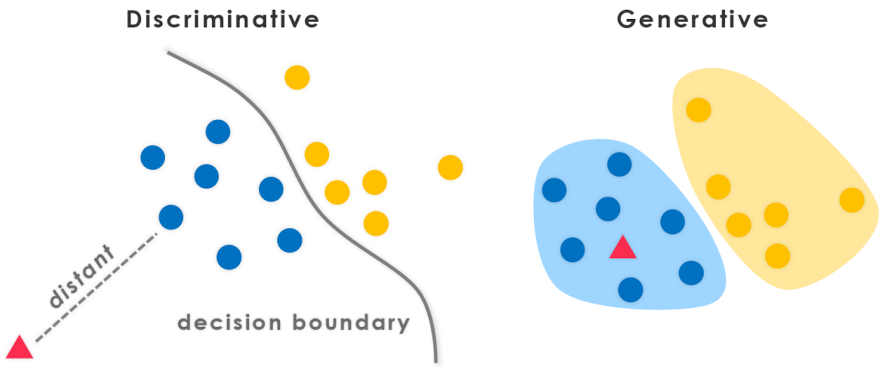

Figure 19: Discriminative vs Generative

uncertainty range of Naive Bayes and HMM, two generative classifiers, is dispersed but concentrates in the middle. A discriminative model focuses on the decision boundary, the difference between each class, whereas the generative model models the actual distribution of each class. The accuracy of detecting anomalies is low due to the inability to consider the data distribution in a discriminative model. In addition, the accuracy scores of both KNN and logistic classifiers are higher than the other two classifiers, which verifies that discriminative classifiers are usually better when applied to classification problems.

Table 4: Comparison among Different Classifiers

	Accuracy	F1-score	Anomaly
Naive Bayes	0.85	0.86	Standard V
KNN	0.96	0.96	Diffused III, Standard V
Logistic	0.95	0.95	Diffused IV, standard V
HMM	0.90	0.90	Diffused V, Standard IV, Standard V

CONCLUSION OF PROJECT

After working on this project, I have realized that to fully understand the whole process of the experiment, tons of papers and research related to background of an industrial field should be done before building a model.

The data wrangling step is crucial to the whole process and without understandable and clean data, the model will do nothing but only 'Garbage in, garbage out'. I have learned many statistical theories and acquired basic knowledge of different statistical models. In the project, I have the chance to put my knowledge in practice and think about how to coherently handle a project. The project is a good start for me for future research. I have thought about how to choose the right model for different situations based on my past study.

In the future, more classifiers such as Decision Tree, Random Forest, and Neural Networks may be applied to compare the accuracy and more anomalies detection methods can be used. Finally, how to integrate multi-scale information such as SEM images will be studied in the future.

REFERENCES

Alberi, Kirstin, Marco Buongiorno Nardelli, Andriy Zakutayev, Lubos Mitas, Stefano Curtarolo, Anubhav Jain, Marco Fornari, Nicola Marzari, Ichiro Takeuchi, Martin L Green, et al. 2018. "The 2019 materials by design roadmap." *J Phys D Appl Phy* 52:013001. doi:https://doi.org/10.1088/1361-6463/aad926.

Aspuru-Guzik, Alán, and Kristin Persson. 2018. *Materials Acceleration Platform: Accelerating Advanced Energy Materials Discovery by Integrating High-Throughput Methods and Artificial Intelligence.* Technical report. doi:http://nrs.harvard.edu/urn-3:HUL.InstRepos:35164974.

Baccar, D, and D Söffker. 2015. "Wear detection by means of wavelet-based acoustic emission analysis." *Mech Sys Signal Proc* 60:198–207. doi:https://doi.org/10.1016/j.ymssp.2015.02.012.

Botcha, Bhaskar, Zimo Wang, Sudarshan Rajan, Natarajan Gautam, Satish TS Bukkapatnam, Amit Manthanwar, Miller Scott, Dean Schneider, and Prakashan Korambath. 2018. "Implementing the Transformation of Discrete Part Manufacturing Systems Into Smart Manufacturing Platforms." In *ASME 2018 13th Int Manuf Sci Eng Conf,* V003T02A009–V003T02A009. ASME. doi:https://doi.org/10.1115/MSEC2018-6726.

Chang, Ding-Chen, and Satish Bukkapatnam. 2004. "Towards characterizing the microdynamics of AE generation in machining." *Mach Sci Tech* 8:235–261. doi:https://doi.org/10.1081/MST-200028743.

Chen, Long-Qing, Li-Dong Chen, Sergei V Kalinin, Gerhard Klimeck, Sanat K Kumar, Jörg Neugebauer, and Ichiro Terasaki. 2015. "Design and discovery of materials guided by theory and computation." *npj Comput Mater* 1:15007. doi:https://doi.org/10.1038/npjcompumats.2015.7.

De Bono, Damaso M, Tyler London, Mark Baker, and Mark J Whiting. 2017. "A robust inverse analysis method to estimate the local tensile properties of heterogeneous materials from nano-indentation data." *Inte J Mech Sci* 123:162–176. doi:https://doi.org/10.1016/j.ijmecsci.2017.02.006.

Iquebal, Ashif S, Shirish Pandagare, and Satish Bukkapatnam. 2019. "Learning acoustic emission signatures from a nanoindentation-based lithography process: Towards rapid microstructure characterization." *Tribology International:* 106074.

Iquebal, Ashif S, Dinakar Sagapuram, and Satish TS Bukkapatnam. 2019. "Surface plastic flow in polishing of rough surfaces." *Sci Rep* 9:10617. doi:https://doi.org/10.1038/s41598-019-46997-w.

Karimi, Navid Zarif, Hossein Heidary, and Mehdi Ahmadi. 2012. "Residual tensile strength monitoring of drilled composite materials by acoustic emission." *Mat Des* 40:229–236. doi:https://doi.org/10.1016/j.matdes.2012.03.040.

Min, Xiao-Hua, Hiroshi Kato, Nobuyuki Narisawa, and Kensuke Kageyama. 2005. "Real-time ultrasonic measurement during tensile testing of aluminum alloys." *Materials Science and Engineering: A* 392 (1-2): 87–93.

Pablo, Juan J de, Barbara Jones, Cora Lind Kovacs, Vidvuds Ozolins, and Arthur P Ramirez. 2014. "The materials genome initiative, the interplay of experiment, theory and computation." *Current Opinion in Solid State and Materials Science* 18 (2): 99–117.

Rabiner, Lawrence R. 1989. "A tutorial on hidden Markov models and selected applications in speech recognition." *Proceedings of the IEEE* 77 (2): 257–286.

Sames, William J, FA List, Sreekanth Pannala, Ryan R Dehoff, and Sudarsanam Suresh Babu. 2016. "The metallurgy and processing science of metal additive manufacturing." *Int Mat Rev* 61:315–360. doi:https://doi.org/10.1080/09506608.2015.1116649.

Sause, MGR, T Müller, A Horoschenkoff, and S Horn. 2012. "Quantification of failure mechanisms in mode-I loading of fiber reinforced plastics utilizing acoustic emission analysis." *Comp Sci Tech* 72:167–174. doi:https://doi.org/10.1016/j.compscitech.2011.10.013.

Wang, Zhuqing, Todd A Palmer, and Allison M Beese. 2016. "Effect of processing parameters on microstructure and tensile properties of austenitic stainless steel 304L made by directed energy deposition additive manufacturing." *Acta Mater* 110:226–235. doi:https://doi.org/10.1016/j.actamat.2016.03.019.

Wei, Qilong, Jiangang Lü, Qiang Yang, and Xiaoyuan Li. 2018. "Multi-pass micro-scratching and tribological behaviors of an austenitic steel in media." *Trib Int* 117:112–118. doi:https://doi.org/10.1016/j.triboint.2017.08.016.

Wisner, Brian, K Mazur, V Perumal, Konstantinos P Baxevanakis, L An, G Feng, and A Kontsos. 2019. "Acoustic emission signal processing framework to identify fracture in aluminum alloys." *Eng Fract Mech* 210:367–380. doi:https://doi.org/10.1016/j.engfracmech.2018.04.027.